J. Fluid Mech. (1998), *vol.* 368, *pp.* 51–79. Printed in the United Kingdom

Experimental investigation of a confined heated sodium jet in a co-flow

By J. U. KNEBEL[1], L. KREBS[1], U. MÜLLER[1] AND B. P. AXCELL[1,2]

[1] Forschungszentrum Karlsruhe GmbH, Institut für Angewandte Thermo- und Fluiddynamik
Postfach 3640, D-76021 Karlsruhe, Germany
j.knebel@iatf.fzk.de
[2] University of Manchester, Department of Engineering, Simon Building,
Manchester M13 9PL, UK

(Received 4 October 1996 and in revised form 24 February 1998)

Low-Prandtl-number convection is investigated in vertical axisymmetric turbulent buoyant sodium jets discharging into a slowly moving ambient. Measurements of mean velocity, mean temperature and temperature fluctuations are performed simultaneously using a miniature permanent-magnet flowmeter probe. By varying the ratio of momentum to buoyancy flux, or the densimetric Froude number, different intensities of buoyancy are obtained giving a range of conditions encompassing forced-convection jets, buoyant jets and plumes. In line with the classical properties of jets the radial velocity and temperature profiles can be described by the Gaussian function, independent of the flow regime, at all axial measuring positions. The axial decay of the centreline mean velocity for sodium is the same as for fluids of higher Prandtl number, governed by power laws with indices of -1 for forced convection, $-2/3$ for the transitional buoyant region and $-1/3$ for plume flow. In contrast, the centreline mean temperatures for sodium plumes decrease with a power of -1 compared with the $-5/3$ decay for fluids of higher Prandtl number. The different behaviour in sodium is due to the dominance of molecular diffusion in heat transport, while momentum transport is dictated by turbulent diffusion, which gives a similarity solution for forced-convection jets but not for buoyant jets or plumes. The radial profiles of the temperature r.m.s. values can be described by an axisymmetric curve with two maxima, independent of the flow regime, at all axial measuring positions and the two maxima are more pronounced than in conventional fluids. The temperature fluctuations are analysed to give statistical parameters such as minimum and maximum values, skewness, flatness, probability density functions and spectral distribution. The spectral distributions display both a convective subrange and the conductive subrange predicted for fluids of low Prandtl number. Integral length scales of the temperature fluctuations are evaluated and found to be significantly smaller than turbulent velocity scales.

1. Introduction

The safety-related removal of decay heat from a liquid metal fast breeder reactor requires knowledge of the flow and temperature fields within the sodium pool under conditions of emergency cooling. Many experiments are performed in small-scale reactor models, see for example Rust *et al.* (1995), and water is often used as the coolant instead of sodium because of fluid dynamic similarity, lower costs and easier

rig operation. This approach creates at least two difficulties. First, the small-scale reactor models can generate laminar mixed convection whereas in the real reactor pool turbulent mixed convection occurs. Second, water has a Prandtl number which is about three orders of magnitude higher than that of sodium. In mixed convection the velocity field depends strongly on the temperature field and the transferability of the results of water experiments to sodium has yet to be proved. Results may be transferred for forced convection, as shown by Krebs & Bremhorst (1983) and Bremhorst *et al.* (1989), but for turbulent mixed convection in a vertical pipe the heat transfer behaviour of sodium is quite different from that of fluids having higher Prandtl numbers, see Jackson, Axcell & Walton (1994).

The buoyant jet flow investigation described in this paper is one of a number being conducted to evaluate the differences between sodium and water. The reason for the different behaviours can be seen from the momentum and energy equations for a buoyant free jet, which, making the Boussinesq approximation, may be written in terms of time mean quantities as

$$u\frac{\partial u}{\partial x}+v\frac{\partial u}{\partial r}=\frac{1}{r}\frac{\partial}{\partial r}\left(r\nu\frac{\partial u}{\partial r}-r\overline{u'v'}\right)+\beta(T-T_a)\,g \tag{1}$$

and

$$u\frac{\partial T}{\partial x}+v\frac{\partial T}{\partial r}=\frac{1}{r}\frac{\partial}{\partial r}\left(r\frac{\nu}{Pr}\frac{\partial T}{\partial r}-r\overline{v'T'}\right). \tag{2}$$

The kinematic viscosity of sodium ν is of a similar order of magnitude to that of water but the Prandtl number is three orders of magnitude lower and this gives a far greater significance to molecular diffusion in the energy equation for sodium. The high thermal conductivity of sodium will therefore cause temperature fluctuations to be damped out more rapidly than in water flow. This differing behaviour is explained theoretically by Batchelor (1959) and Batchelor, Howells & Townsend (1959). They find that the spectrum of temperature fluctuations decays at a rate proportional to wavenumber to the power $-17/3$ in a fluid of low Prandtl number in a conduction subrange. This subrange is not present in fluids of moderate or high Prandtl number where the decay is less rapid.

The vertical axisymmetric buoyant jet is chosen for study as it has been reported extensively in the literature, the first measurements having been made in air 50 years ago by Corrsin (1943) and Corrsin & Uberoi (1949). A comprehensive review of buoyant jets is given by Chen & Rodi (1975, 1980), who, following the approach of Ricou & Spalding (1961), divide buoyant jets into three regions using general scaling laws. They distinguish the two asymptotic cases of the pure isothermal jet and the pure plume and from dimensional reasoning they derive similarity laws for the axial decay of velocity and temperature. They also define a transition region which does not show similarity and which is described by empirical laws.

Ogino *et al.* (1980) report a large number of buoyant jet experiments in water spanning all the three regions and confirming the decay laws and empirical constants given by Chen & Rodi (1980). List (1982*a*, *b*), following the approach of Morton (1959) and Baker, George & Taulbee (1982), gives a characteristic length scale which defines the distance from the origin at which buoyancy forces become important. Using this length scale to classify buoyant jets, Papanicolaou & List (1987, 1988) investigate the decay behaviour of the velocity and the temperature or concentration fields. In addition, they measure the probability density function and higher-order moments such as skewness and flatness, which allow a clear distinction to be made between jets which are influenced by buoyancy and those which are not. More recently, experimental

work on turbulent mixing in jets is reported by Dahm & Dimotakis (1990) for a large but unspecified Schmidt number and by Dowling & Dimotakis (1990) for a more moderate Schmidt number. The effect of variable density on jet behaviour is studied experimentally by Richards & Pitts (1993) and theoretically by Ruffin *et al*. (1994) but both investigations are restricted to the inertial regime. Ruffin *et al*. (1994) use a Reynolds stress model to gain information about mean flow values and turbulence parameters and they compare their predictions with a wide range of experimental data.

The properties of liquid sodium place great restrictions on the design of experimental apparatus and the choice of instrumentation. Liquid sodium reacts explosively with water, it catches fire when exposed to air and it is highly corrosive with many materials. Temperature measurements can be made in sodium using thermocouples provided that the thermoelements are sheathed in stainless steel or another suitable material. Because of the very high heat transfer coefficients that are characteristic of liquid sodium the frequency response of thermocouples in sodium is far higher than in conventional fluids. According to Krebs & Bremhorst (1983) a 0.25 mm sheathed thermocouple with an insulated junction gives undamped signals in excess of 40 Hz.

Velocity measurements in sodium are not possible using conventional techniques such as Pitot tubes, hot-film anemometers and optical devices. Transit time techniques have been used for velocity measurement, see Reimche, Stegemann & Montes (1985) and Horanyi & Krebs (1986). The use of ultrasonics has been proposed by Takeda (1986) although the non-availability of high-temperature transducers has prevented the implementation of the technique. The most successful approach to date, and the most widely used, is the magnetic method, see Müller & Thun (1980), Ricou & Vives (1982), von Weissenfluh (1985), Shercliff (1987) and Walton (1991). A miniature permanent-magnet flowmeter probe (MPMF probe) has been developed at the Forschungszentrum Karlsruhe, the working principle of which is based on electromagnetic induction. The first velocity measurements made using it are reported by Horanyi & Krebs (1988) and Bremhorst & Krebs (1989, 1992), resolving mean velocities of between 0.1 m s^{-1} and 1.3 m s^{-1} with a weak temperature gradient present. Axcell & Walton (1993) improve the calibration of the probe, but leave some unresolved nonlinearities of the signals for velocities below 0.1 m s^{-1}. By changing the electrode material of the probe to stainless steel Knebel & Krebs (1993, 1994) succeed in producing a flowmeter probe which combines sensitivity to low velocities and signal stability while minimizing thermo-electric effects. The probe enables simultaneous measurements of mean velocity and mean and fluctuating temperature to be obtained (Knebel 1993; Knebel, Krebs & Müller, 1993; Knebel & Krebs 1994).

Because of the difficulties in measuring fluid velocities the emphasis of sodium heat transfer experiments is often the correlation of heat transfer coefficients. A number of investigators also attempt to evaluate the eddy diffusivity of heat, for example Fuchs (1972) and Sheriff & O'Kane (1981). Bunschi (1976) reports temperature measurements in a heated sodium pipe and gives statistical information about the turbulence which confirms the division of the power spectral density into a convective subrange and a conduction subrange with characteristic decays as predicted by Batchelor *et al*. (1959) for fluids of very low Prandtl number.

The present investigation goes somewhat further: simultaneous measurements of velocity, temperature and fluid temperature fluctuations are reported for a sodium jet emerging into a confined co-flowing stream. The apparatus, experimental conditions and instrumentation are described in the following two sections. The experimental results are then compared with the extensive data available for isothermal jets, buoyant jets and plumes in fluids of higher Prandtl number. The differences are discussed and

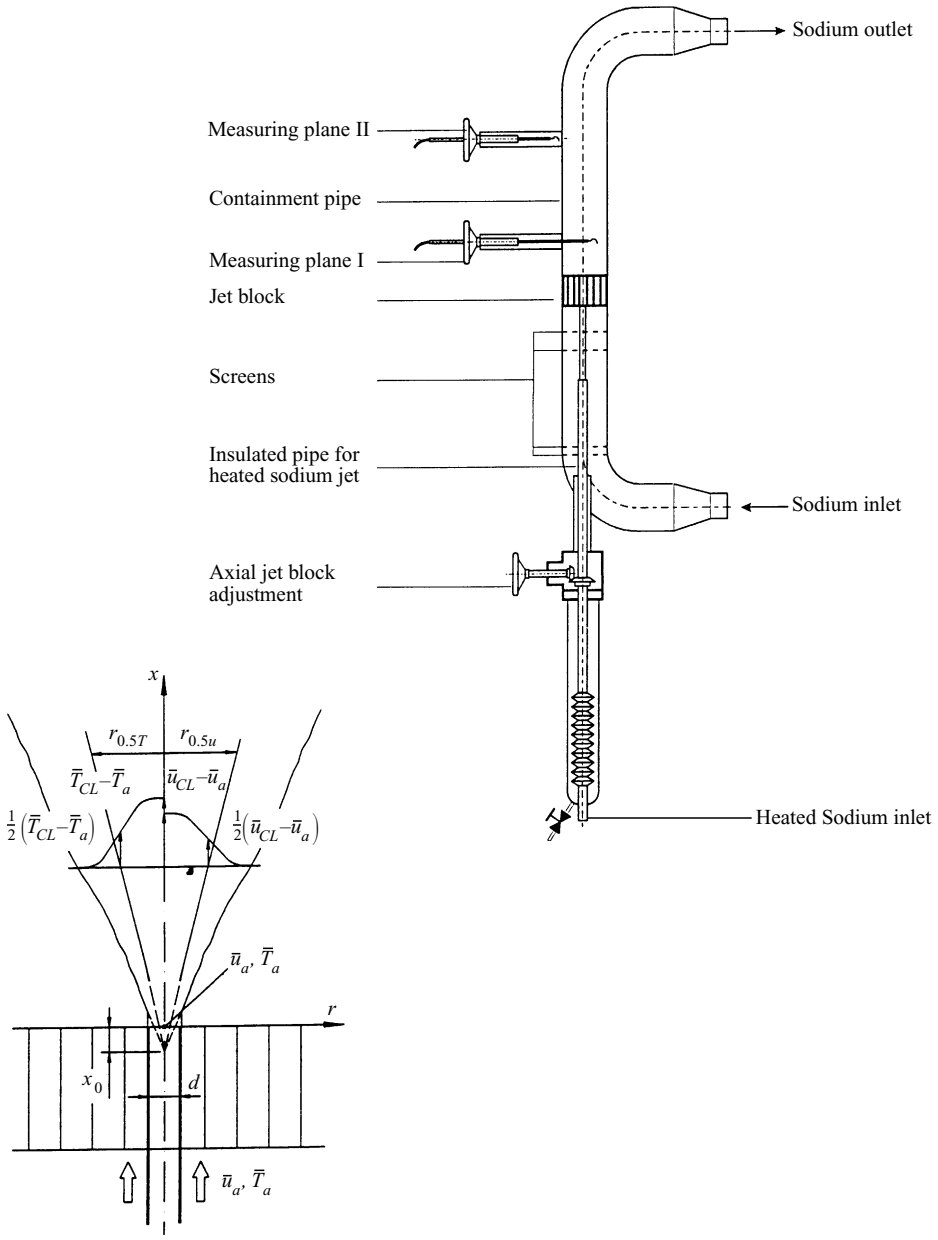

FIGURE 1. Sketch of the sodium test section TEFLU and flow configuration.

the separate influences of jet confinement, the co-flowing stream and the high fluid conductivity considered.

2. Apparatus and experimental conditions

The experimental data are obtained in the sodium test section TEFLU, figure 1, consisting essentially of a vertical pipe of 110 mm inner diameter and an axially movable jet block. Two measurement positions are provided at different axial positions but only the lower position is used in this study. Probes can be traversed across a

	Isothermal jet	Forced-convection jet	Buoyant jet in the transition regime	Plume
Reynolds number, Re_a	1.4×10^4	1.4×10^4	2.8×10^4	2.8×10^4
mean main flow velocity, $\bar{u}_a$	0.05 m s^{-1}	0.05 m s^{-1}	0.10 m s^{-1}	0.10 m s^{-1}
mean main flow temperature, $\bar{T}_a$	300 °C	300 °C	300 °C	300 °C
densimetric Froude number, Fr_0	8123	521	365	43.1
mean initial excess velocity, $\Delta\bar{u}_0$	0.48 m s^{-1}	0.50 m s^{-1}	0.33 m s^{-1}	0.17 m s^{-1}
mean initial excess temperature, $\Delta\bar{T}_0$	1.8 K	30 K	25 K	75 K
axial distances, x/d	3, 4, 6, 8, 12, 20, 30	3, 4, 6, 8, 10, 12, 15, 20, 25, 30, 35, 40	3, 4, 6, 8, 12, 20, 30, 40	3, 4, 6, 8, 12, 20, 30, 40

TABLE 1. Experimental conditions.

diameter of the pipe, the accuracy of the radial adjustment being 0.1 mm. The jet block can be adjusted between axial distances x of 10 mm and 500 mm from the lower measurement position, allowing the measurement of radial temperature and velocity profiles for normalized distances x/d between 1.4 and 70. The jet block contains 158 holes of diameter $d = 7.2$ mm located on a triangular pitch of 8.2 mm, and the holes have a length-to-diameter ratio of 16.7.

The temperature of the co-flow in the pipe is 300 °C. A sodium jet, heated to as much as 75 K above the co-flow temperature, is injected separately into the central hole of the jet block, which also has a diameter of $d = 7.2$ mm. The velocity at the orifice of the nozzle is varied between 0.27 and 0.55 m s^{-1}, corresponding to a Reynolds number range of about 5×10^3 to 10^4. The central injection pipe is double-walled with an evacuated annular gap. The uppermost 170 mm of the central pipe is also of 7.2 mm internal diameter and so the jet exit conditions correspond to a fully developed turbulent velocity profile at a uniform temperature.

Without any co-flow the physical confinement would generate significant return flows outside the jet to satisfy the conservation of mass (the ratio of the pipe diameter to the jet outlet diameter is only 15). The model of Hussein, Capp & George (1994) suggests that in the present experimental apparatus jet momentum would be conserved for only a few jet outlet diameters downstream of the jet block. In addition, the stagnant sodium along the pipe wall would cool down due to heat losses across the wall, possibly causing a thermally induced flow reversal. In order to prevent such a flow reversal near the wall, the Reynolds number of the co-flow is kept at $Re_a = 1.4 \times 10^4$ for the forced convection jet. Because the loop characteristics prevent steady conditions in the central pipe at low flow rates and high initial temperature differences the Reynolds number of the co-flow is kept at $Re_a = 2.8 \times 10^4$ for the buoyant jet and the plume experiments. These pipe Reynolds numbers, formed using the velocity of the co-flow and the diameter of the pipe, correspond to co-flow velocities of 0.05 and 0.10 m s^{-1}, respectively. The experimental conditions do not generate recirculation, as shown by measurements in the pipe outside the central jet which reveal uniform velocities right up to a thin boundary layer at the pipe wall. The Craya–Curtet number is in excess of 1.5 for all tests carried out, see Steward & Guruz (1977).

Three different series of measurements are performed as listed in table 1. The initial

character of the jet (subscript 0) is specified by the densimetric Froude number Fr_0 at the orifice of the nozzle, which may be regarded as the ratio of inertial forces to buoyancy forces. It is defined as

$$Fr_0 = \frac{\rho_0(\bar{u}_0^2 - \bar{u}_a^2)}{g(\rho_a - \rho_0)\, d}, \tag{3}$$

where $\bar{u}_0$ and $\bar{u}_a$ are respectively the mean velocities at the orifice of the nozzle and of the co-flow and ρ_0 and ρ_a are respectively the densities of the heated jet and the co-flow.

3. Instrumentation and measurement accuracy

The temperature-compensated miniature permanent-magnet flowmeter probe (MPMF probe) is shown schematically in figure 2. It consists essentially of a stainless steel sheath of outer diameter 2.5 mm which contains a miniature AlNiCo 450 permanent magnet, of length to diameter ratio 1 and magnetized radially. The measuring principle is based on electromagnetic induction: liquid sodium flows in a vertical direction through a horizontal magnetic field, generating an electromotive force (e.m.f.) which is perpendicular to both the liquid sodium flow and the magnetic field and proportional to the sodium velocity. The e.m.f. is detected using grounded thermocouples 0.25 mm in diameter which are welded onto the sheath of the probe normal to the permanent magnet poles at positions 1 and 2 (lower probe plane). The e.m.f. is measured between two thermocouple wires of the same material that are marked *A* (Alumel), *C* (Chromel) or *S* (stainless steel). The thermocouples are routed inside the probe sheath. If a temperature field is superimposed on the velocity field, a thermoelectric voltage is added to the velocity-induced voltage. In order to compensate for the thermoelectric voltage two other grounded thermocouples are installed at positions 3 and 4 (upper probe plane) and these are only weakly influenced by the magnetic field. The distance between the two probe planes is 3.0 mm. An additional thermocouple of 0.25 mm diameter at the tip of the probe (position 5) is used for measuring the mean temperature and the temperature fluctuations. The distance between the thermocouple position 5 and the lower probe plane is equal to the jet diameter *d*.

The MPMF probe design allows the simultaneous measurement of the temperatures at the five thermocouple positions and of the three voltages at each probe plane, i.e. U_{21A}, U_{21C}, U_{21S}, U_{43A}, U_{43C} and U_{43S}. The voltmeters used have a resolution of 0.1 μV and an adjustable integration time of multiples of 10 s. The probe responds very rapidly to changes in velocity but long integration times are needed to establish accurate mean values of the very low voltages. The temperature fluctuations are first measured with an integrating RMS-voltmeter which gives the r.m.s. values. Then, in a separate measurement, the time history of the temperature fluctuations is recorded over a frequency range from 0.1 Hz to typically 500 Hz, the latter figure being chosen because it is sufficiently higher than the frequency response of the probe to avoid a loss of information about the frequency spectrum.

In the following paragraphs the velocity measurement will be explained briefly (a detailed explanation is given by Knebel & Krebs 1994). The voltages consist of components depending on the velocity and temperature:

$$U_{21A,C,S} = E_{21} + (S_{A,C,S} - S^*_{N21})\,\Delta T_{21} \tag{4}$$

in the lower probe plane, and

$$U_{43A,C,S} = \alpha E_{21} + (S_{A,C,S} - S^*_{N43})\,\Delta T_{43} \tag{5}$$

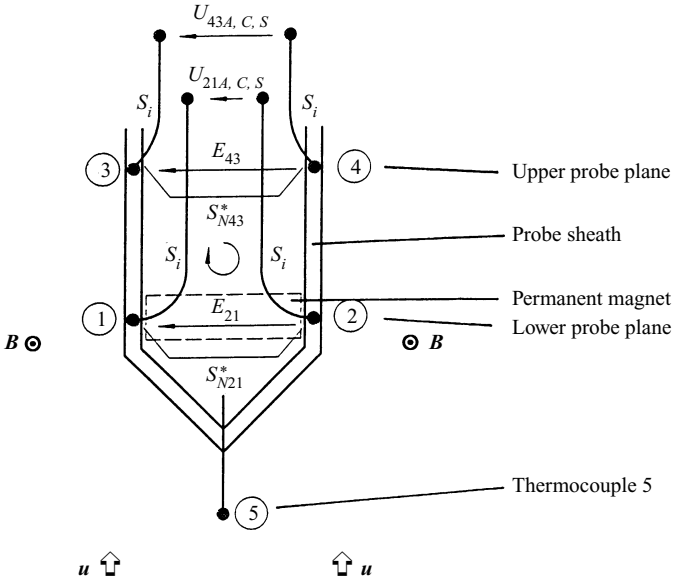

FIGURE 2. Sketch of the temperature-compensated miniature permanent-magnet flowmeter probe (MPMF probe). Outer probe diameter 2.5 mm.

in the upper probe plane. E_{21} is the velocity-induced voltage in the lower probe plane, a is the ratio of the velocity-induced voltages at the two probe planes, $S_{A,C,S}$ are the Seebeck coefficients corresponding to the materials of the thermocouple wires, and ΔT_{21} and ΔT_{43} are the temperature differences in the lower and the upper probe planes respectively. S^*_{N21} and S^*_{N43} are the Seebeck coefficients of the electrically conductive connections between the two thermocouple positions at the two probe planes and these depend on the Seebeck coefficients of the sodium and the stainless steel and the relative electrical resistances of the paths through the sodium and the stainless steel. Assuming identical Seebeck coefficients S^*_{N21} and S^*_{N43} the velocity-induced voltage E_{21} can be determined by the measurement of four voltages. Equations (4) and (5) for Alumel and stainless steel give

$$E_{21} = \frac{U_{43A}\,U_{21S} - U_{21A}\,U_{43S}}{U_{43A} - U_{43S} + \alpha(U_{21S} - U_{21A})}. \tag{6}$$

It should be noted that Chromel has a very high Seebeck coefficient relative to Alumel and stainless steel and hence the voltages U_{21A}, U_{21S} and U_{43A}, U_{43S} are preferred for the evaluation of the velocity signal instead of U_{21C} and U_{43C} because thermoelectric effects are smaller.

Alternatively the voltage induced by the sodium velocity may be calculated from

$$E_{21} = \frac{U_{21A} - K_{AS}\,U_{21S}}{1 - K_{AS}}, \tag{7}$$

where

$$K_{AS} = \frac{S_A - S^*_{N21}}{S_S - S^*_{N21}}. \tag{8}$$

This means that only two voltages have to be measured to obtain the sodium velocity but K_{AS} has to be found by calibration.

The sensitivity of the probe is determined by calibration and mean sensitivities of about 47 μV/(m s^{-1}) are obtained for MPMF probes of 2.5 mm outer diameter. According to Müller & Thun (1977) the spatial resolution of the probe is equal to twice the diameter of the MPMF probe, or 5.0 mm, although the MPMF probe gives a varying output when moved much smaller distances in velocity gradients. The probe signal reflects the average velocity of the sodium flowing over it and provided that the velocity distribution across the probe diameter is approximately linear an accurate velocity profile will be obtained. Knebel & Krebs (1994) present a velocity profile for an axial position close to the jet outlet ($x/d = 4$) where the velocity variation is restricted to a radial distance of less than 20 mm, but the profile is still in good agreement with the theoretical Gaussian curve. The limiting accuracy is on the jet axis where the rapid changes in velocity around the maximum may not be captured fully.

The experimental data consist of time-mean velocities, time-mean temperatures and the intensity of the temperature fluctuations. Information on Reynolds stresses and turbulent heat fluxes would also be of interest but the sensitivity of the probe is not sufficient to resolve the low levels of the velocity fluctuations. The 2.5 mm diameter MPMF probe, although warranting the description of miniature when compared with conventional sodium instrumentation, is also too large when compared with the scale of the turbulence. The 0.25 mm diameter of the thermocouple used for temperature measurement will be shown to be small enough to capture the significant temperature fluctuations in the liquid sodium.

The accuracy of the velocity measurement depends on the zero offsets for the probe signals, which have to be constant for a long time, and on the stability of the voltmeters. Both zero offset and voltmeter drift are small compared with the signal itself. The probe offsets are determined before each measurement by calibration (Knebel & Krebs 1994) and this procedure gives an accuracy of $\pm 7\%$ for sodium velocities above 0.05 m s^{-1}, even with temperature gradients of more than 10 K mm^{-1}.

Parallel to the sodium velocity and temperature measurement, the following data for the sodium loop are recorded with a data-logger and used in evaluating the co-flow temperature and volume flow rate: the temperature and volume flow rate of the heated jet and the radial measurement position r for the MPMF probe. The resolution of the data-logger is 1 μV which is sufficient for this application. The temperatures of the co-flow and the jet flow are controlled to within 0.2 K/day by an online microcomputer. The two volume flow rates are measured by separate electromagnetic flowmeters, each with an accuracy of about $\pm 1.5\%$, and they can be regulated independently of one another.

4. Experimental results and discussion

4.1. *Dimensionless numbers and parameters*

The initial conditions of the different measurements are chosen according to the Froude numbers shown in table 1. In the following figures data for the isothermal jet will be marked using an asterisk (*), data for the forced-convection jet using a square (□), data for the buoyant jet using a triangle (△) and data for the plume using a circle (○). At each axial position the MPMF probe is moved across the pipe over the range $-35 \leqslant r \leqslant +35$ mm taking data points every millimetre. The temperature measurement is performed using thermocouple number 5 shown in figure 2 which is located one jet diameter upstream of the lower probe plane where the mean velocity is measured. Thus, the locations of the temperature and the velocity measurements are a normalized distance $x/d = 1$ apart.

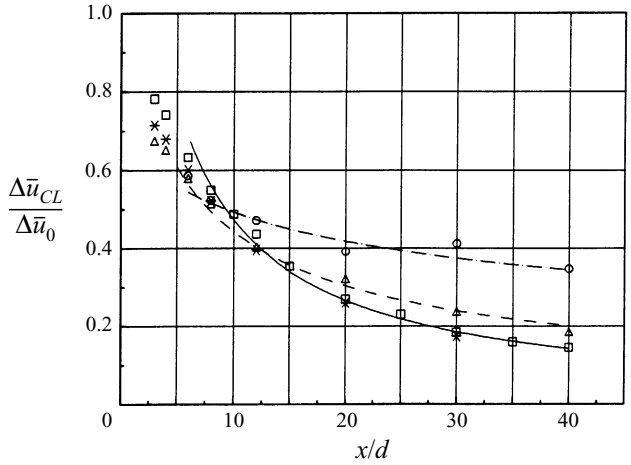

FIGURE 3. Excess mean centreline velocity versus distance from the orifice. *, Isothermal jet; □, forced-convection jet, ——, equation (9); △, buoyant jet, – – –, equation (10); ○, plume, –·–·–, equation (11).

4.2. *Mean velocity and mean temperature*

The mean velocity and the mean temperature are always given relative to the values in the co-flow, see figure 1. Figure 3 shows the decay of the excess centreline velocity $\Delta\bar{u}_{CL}/\Delta\bar{u}_0$ versus the distance x/d from the orifice.

Beyond a zone of flow establishment which finishes at about $x/d = 6$ the decay of the mean centreline velocity can be described by the following equations:

$$\frac{\Delta\bar{u}_{CL}}{\Delta\bar{u}_0} = 6.08\left(\frac{x}{d}+2.84\right)^{-1} \tag{9}$$

for the isothermal jet and the forced convection jet,

$$\frac{\Delta\bar{u}_{CL}}{\Delta\bar{u}_0} = 6.62\,Fr_0^{-1/6}\left(\frac{\rho_0}{\rho_a}\right)^{5/12}\left(\frac{x}{d}+3.17\right)^{-2/3} \tag{10}$$

for the buoyant jet in the transition region, and

$$\frac{\Delta\bar{u}_{CL}}{\Delta\bar{u}_0} = 4.32\,Fr_0^{-1/3}\left(\frac{x}{d}+5.61\right)^{-1/3} \tag{11}$$

for the plume.

The Froude number dependences are taken from Chen & Rodi (1975). The exponents of -1 and $-1/3$ in equations (9) and (11) are in agreement with the exponents obtained by Chen & Rodi (1980) in their similarity analysis. The decay factor of $A_u = 6.08$ for the isothermal jet and the forced-convection jet is consistent with the values of 6.2 and 5.8 given in the reviews of Chen & Rodi (1980) and Ogino *et al.* (1980), respectively, and within the range reported by Ruffin *et al.* (1994) and this demonstrates that the flow is dominated by inertial forces. Identical measurements by Knebel & Krebs (1994) in a forced-convection jet with an initial Froude number of $Fr_0 = 521$, which were made about nine months before the present investigations, give a decay factor of $A_u = 6.25$, thus proving the reproducibility of the measurements and the long-term stability of the MPMF probe.

Buoyancy forces are of great importance for the plume flow and they produce a

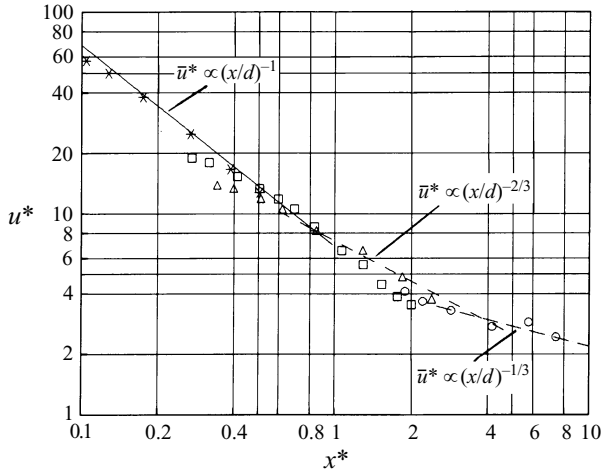

FIGURE 4. Dimensionless centreline velocity versus non-dimensionalized distance from the orifice. *, Isothermal jet; □, forced-convection jet; △, buoyant jet; ○, plume.

much slower decay along the centreline as the thermal energy in the plume is transformed into kinetic energy. The decay factor of $B_u = 4.32$ in equation (11) is in reasonable agreement with the values of $B_u = 3.5$, 3.4 and 3.4 given by Chen & Rodi (1980), Shabbir & George (1994) and Ogino *et al.* (1980) respectively and with the somewhat higher values of $B_u = 3.89$ and 3.85 given by Nakagome & Hirata (1977) and Papanicolaou & List (1988), respectively. The data points of the buoyant jet lie between the other two curves and they can be described by an empirical power law with a decay factor of 6.62.

The mean centreline velocity and the distance from the orifice are now expressed in the dimensionless form first proposed by Ricou & Spalding (1961):

$$\bar{u}^* = \frac{\Delta\bar{u}_{CL}}{\Delta\bar{u}_0} Fr_0^{1/2} \left(\frac{\rho_0}{\rho_a}\right)^{-1/4} \left(\frac{\pi}{4}\right)^{-1/4}, \tag{12}$$

$$x^* = \left(\frac{x}{d} - \frac{x_0}{d}\right) Fr_0^{-1/2} \left(\frac{\rho_0}{\rho_a}\right)^{-1/4} \left(\frac{\pi}{4}\right)^{-1/4}. \tag{13}$$

Using this scaling, figure 4 allows the identification of three regions with different characteristics, which can be distinguished by the value of x^* depending on the distance from the orifice and the Froude number at the orifice. For values of $x^* \leqslant 0.8$ the flow behaves like an isothermal jet. Within a range of about $0.8 \leqslant x^* \leqslant 5.0$ a transition takes place, at the end of which the flow is completely controlled by buoyancy forces so that for $x^* \geqslant 5.0$ the jet behaves like a pure plume. The transitional range is consistent with those defined by Chen & Rodi (1980) and Ogino *et al.* (1980) and it covers the transitional range investigated by Panchapakesan & Lumley (1993*b*). The data of Shabbir & George (1994) are in the range $7.56 \leqslant x^* \leqslant 26.4$ and are thus in the pure plume region.

Figure 5 gives the decay of the excess centreline temperature $\Delta\bar{T}_{CL}/\Delta\bar{T}_0$ versus the distance x/d from the orifice. All measurements show a temperature decay proportional to $(x/d - x_0/d)^{-1}$ regardless of the initial Froude number:

$$\frac{\Delta\bar{T}_{CL}}{\Delta\bar{T}_0} = A_T \left(\frac{x}{d} - \frac{x_0}{d}\right)^{-1}. \tag{14}$$

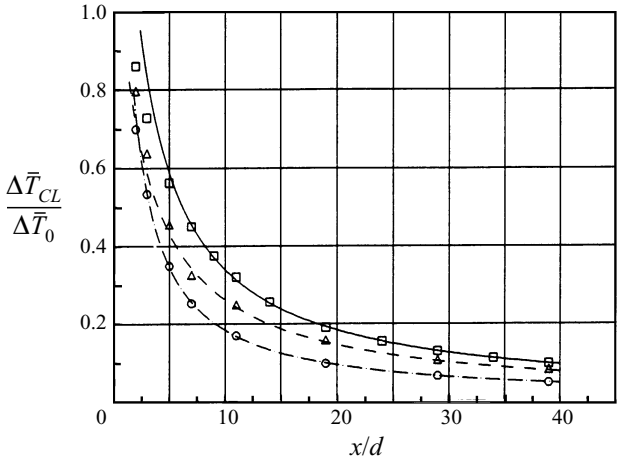

FIGURE 5. Excess mean centreline temperature versus distance from the orifice. □, Forced convection jet, ——, equation (14) and $A_T = 4.01$; □, buoyant jet, – – –, equation (14) and $A_T = 3.3$; ○, plume, –·–·–, equation (14) and $A_T = 1.95$.

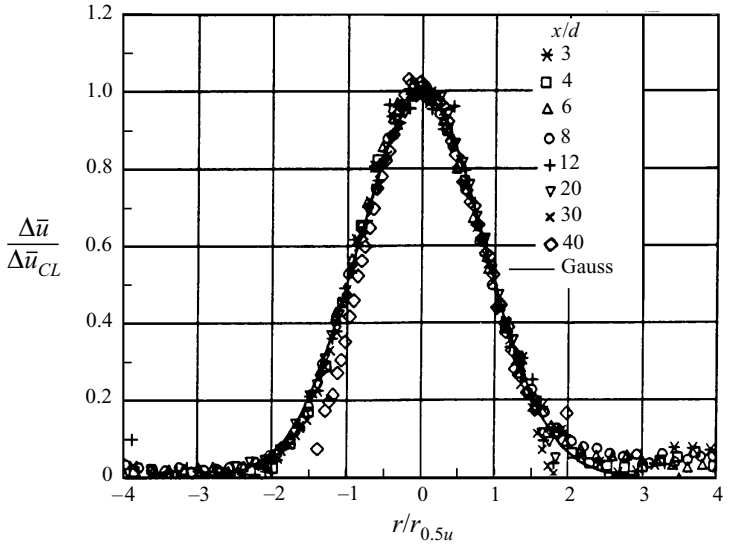

FIGURE 6. Radial velocity profile: forced-convection jet. ——, Gaussian function, equation (15).

The only distinction between the different measurements is the decay factor A_T which decreases with decreasing Froude number. The decay factor is found to be 4.01 for the forced convection jet, 3.3 for the buoyant jet and 1.95 for the plume with virtual origins of $x_0/d = -0.55$, -2.6 and -0.65 respectively. The reason for this behaviour is that the absolute axial velocity decreases with decreasing Froude number. Each element of sodium remains longer in a particular x/d-section, thus allowing molecular diffusion to transport more thermal energy in the radial direction and giving smaller values of A_T. Even the value of A_T for the forced-convection jets is at the lower end of the range of 4 to 6 quoted by various authors for turbulent mixing in jets (see, for example, Dahm & Dimotakis 1990; Dowling & Dimotakis 1990; Richards & Pitts 1993; and Ruffin *et al.* 1994); this low value is almost certainly due to the prominent role of molecular

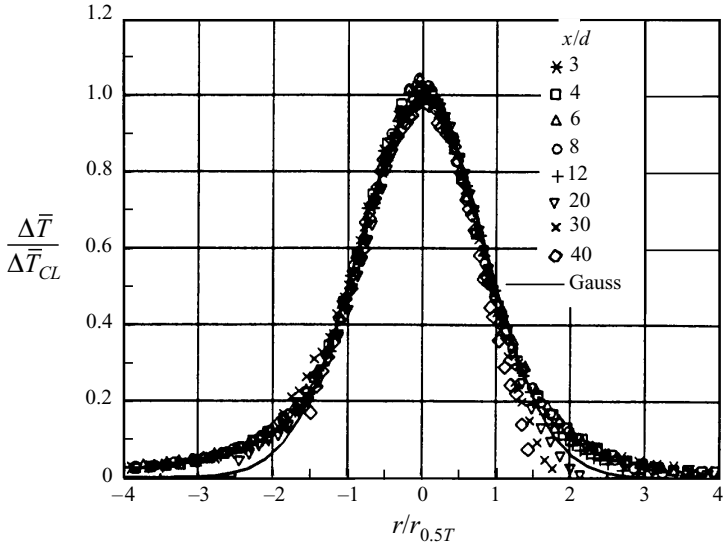

FIGURE 7. Radial temperature profile: forced-convection jet. ——, Gaussian function, equation (16).

diffusion. The behaviour in sodium is in contrast to similar experiments employing fluids of higher Prandtl number, where at least two different decay laws are needed to fit the experimental data. A decay proportional to $(x/d)^{-5/3}$, which is found for plumes in fluids of higher Prandtl number, is not observed for the range of Froude numbers investigated.

Figures 6 and 7 respectively show the mean velocity and temperature profiles $\Delta\bar{u}/\Delta\bar{u}_{CL}$ and $\Delta\bar{T}/\Delta\bar{T}_{CL}$, both relative to conditions in the co-flow, see figure 1, and normalized by the centreline values. The radius is normalized using the characteristic half-value radii $r_{0.5u}$ and $r_{0.5T}$ for the velocity and the temperature profiles, respectively. Figures 6 and 7 give eight profiles for a forced-convection jet and these are representative of all the measurements made. All data are correlated by a single curve, described by the Gaussian function

$$\frac{\Delta\bar{u}}{\Delta\bar{u}_{CL}} = \exp\left(-\ln 2\left(\frac{r}{r_{0.5u}}\right)^2\right), \tag{15}$$

$$\frac{\Delta\bar{T}}{\Delta\bar{T}_{CL}} = \exp\left(-\ln 2\left(\frac{r}{r_{0.5T}}\right)^2\right). \tag{16}$$

The profiles are axisymmetric and they have the same shape for all the distances investigated. Thus, the mean values of the flow show self-preservation. Temperatures are slightly higher than predicted by the Gaussian function for radii of $|r/r_{0.5T}| > 1.3$, due to the high thermal conductivity of sodium which causes a diffusion of heat farther into the co-flow.

Figure 8 gives the half-value radii of the velocity profiles $2r_{0.5u}/d$, which are obtained by fitting the Gaussian profile of equation (15) to the velocity data, as a function of axial distance. The experimental half-value radii are described well by

$$\frac{2r_{0.5u}}{d} = 2S_u\left(\frac{x}{d} - \frac{x_0}{d}\right) \tag{17}$$

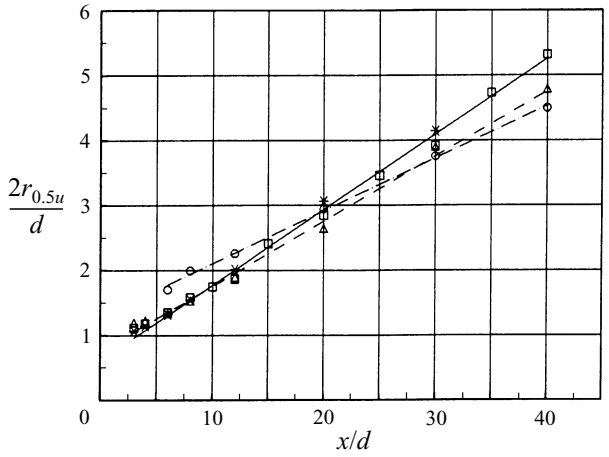

FIGURE 8. Half-value radii of velocity profiles versus distance from virtual origin. *, Isothermal jet; □, forced-convection jet, ——, equation (17) and $S_u = 0.058$; △, buoyant jet, – – –, equation (17) and $S_u = 0.048$; ○, plume, –·–·–, equation (17) and $S_u = 0.041$.

with S_u being the rate of velocity spread. Fitting the data points by a least-squares procedure gives a linear spreading of the mean velocity for all the measurements made, with values of S_u of 0.058 for the isothermal jet and the forced-convection jet, 0.048 for the buoyant jet and 0.041 for the plume. The virtual origins x_0/d are -5.24, -7.87 and -15.9 respectively. The value of S_u for an isothermal jet is lower than the value of 0.096 given by Panchapakesan & Lumley (1993*a*), the 0.08–0.1 range reported by Ruffin *et al.* (1994) or the value of 0.086 recommended by Chen & Rodi (1980), due to the confining effects of the co-flow.

The data suggest that the mean velocity profile in sodium spreads faster for an isothermal jet than for a plume. The strong velocity increase due to buoyancy effects results in a strong axial momentum flux just where high excess temperatures are present (the momentum flux will be discussed later); this effect could tend to hold the buoyant jet together and to diminish the rate of spread compared to an isothermal jet. Alternatively, buoyancy could result in a greater entrainment and hence a wider jet. A comparison with measurements in fluids of higher Prandtl number is equivocal: Papanicolaou & List (1988) confirm the observations of the sodium experiments, Chen & Rodi (1980) and Panchapakesan & Lumley (1993*b*) report the opposite behaviour. It should be noted that in the present investigation the co-flow velocity is larger for the buoyant jet and the plume than for the isothermal jet and the forced-convection jet, both in absolute terms and relative to the jet exit velocity. The higher co-flow velocity will tend to reduce the spreading of the jet and it will be seen later that the co-flow has a greater impact than buoyancy in this respect.

The half-value radii of the temperature profiles $2r_{0.5T}/d$ are also obtained by fitting a Gaussian profile (equation (16)) to the temperature data, and figure 9 shows their variation with distance x/d from the orifice. Up to $x/d = 19$ all the data are described well by

$$\frac{2r_{0.5T}}{d} = 2S_T\left(\frac{x}{d} - \frac{x_0}{d}\right) \tag{18}$$

with S_T being the rate of temperature spread. A least-squares procedure for the forced-convection jet data results in a rate of temperature spread of 0.077, the virtual origin

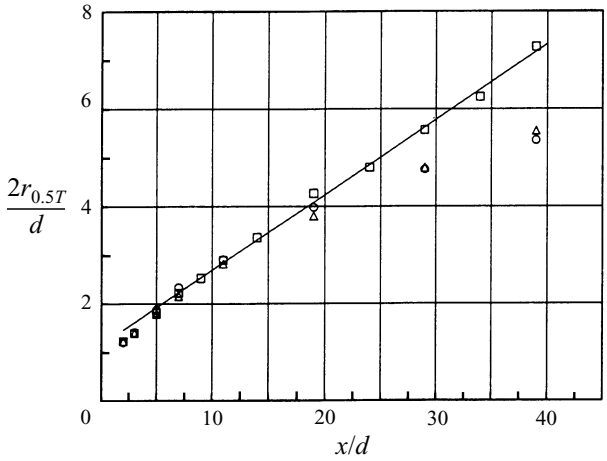

FIGURE 9. Half-value radii of temperature profiles versus distance from the orifice. □, Forced-convection jet, ——, equation (18) and $S_T = 0.077$; △, buoyant jet; ○, plume.

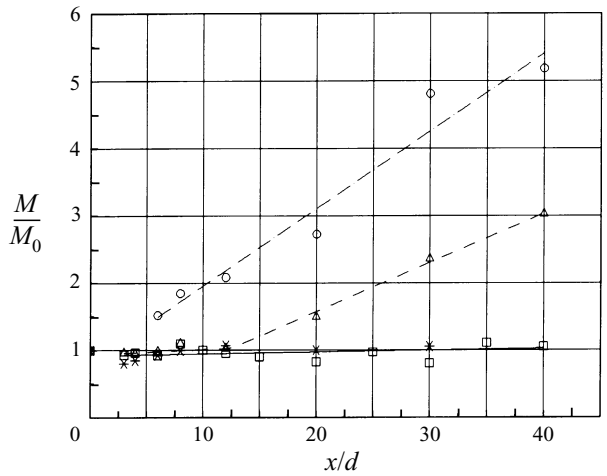

FIGURE 10. Momentum flux versus distance from the orifice. *, Isothermal jet; □, forced-convection jet; △, buoyant jet; ○, plume.

x_0/d being -7.41. The value of S_T is again less than the spreading rates quoted in the literature for free jets. Chen & Rodi (1980) suggest a value of 0.11 and this is consistent with the data of Dowling & Dimotakis (1990) and Richards & Pitts (1993) and within the range of values of 0.1 to 0.12 reported by Ruffin *et al.* (1994). For greater distances with the buoyant jet and the plume there is a noticeable influence of buoyancy on the flow with the half-value radii of the temperature profiles increasing less than that of the forced-convection jet. Furthermore, the development is not linear. The increase of the axial momentum flux due to buoyancy forces causes an increased transport of heat in the axial direction and this results in a weaker rate of temperature spread. The trend is confirmed by Papanicolaou & List (1988), Chen & Rodi (1980) and Shabbir & George (1994) for fluids of higher Prandtl number.

The momentum flux M relative to the co-flow can be calculated by means of the velocity profiles. The normalized momentum flux M/M_0, with M_0 being the initial momentum flux, is given in figure 10 for all the measurements made. The momentum

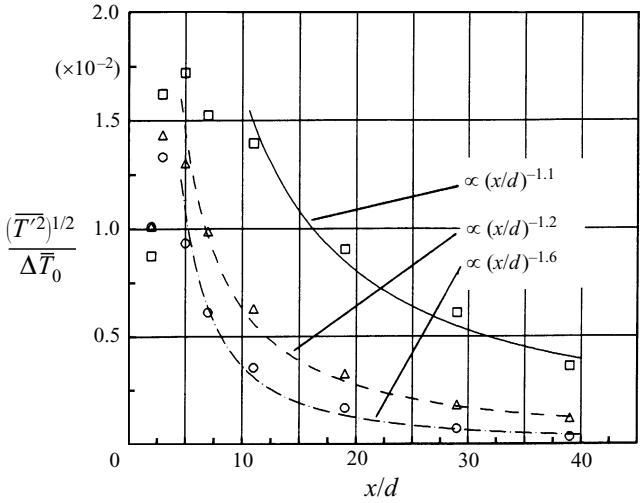

FIGURE 11. Centreline temperature r.m.s. values versus distance from the orifice. □, Forced-convection jet; △, buoyant jet; ○, plume.

fluxes of the isothermal jet and the forced-convection jet show nearly constant values within the x/d range investigated, a least-squares procedure giving a slope of 0.0027. Ricou & Spalding (1961) state that in the case of a pure jet discharging into a stagnant ambient with zero pressure gradient, the momentum flux is equal to the initial momentum flux for all axial distances. A pure jet in a co-flowing ambient, however, has a slightly increasing momentum flux with increasing distance from the orifice, according to Taylor (1958) and Fischer *et al.* (1979), because of the momentum of the entrained fluid. In the case of an isothermal jet which discharges into a stagnant ambient limited by walls, Schneider (1985) deduces theoretically a decreasing momentum flux. This is explained by a recirculation of the ambient fluid that is induced by the jet itself. The above statements are summarized by Kotsovinos & Angelidis (1991) who prove all three to be theoretically possible. The relevant parameter is the angle at which a co-flowing ambient or an induced recirculation enters the jet. With the co-flowing ambient in the present sodium experiments there appears to be a slight increase in the momentum flux of the isothermal jet with axial distance.

As shown in figure 4, the momentum flux of the buoyant jet remains approximately constant up to a distance of $x/d = 12$ which corresponds to the transitional value of $x^* = 0.8$. Beyond this distance buoyancy forces have an appreciable influence and the momentum flux increases linearly with a slope of 0.073 as potential energy, which is stored in the buoyant jet in the form of density differences relative to the ambient fluid, is transformed into kinetic energy. As expected, the plume shows the largest increase in momentum flux because of the high initial buoyancy and the increase commences very nearly at the orifice. A least-squares procedure for the data gives a slope of 0.115.

4.3. *Temperature fluctuations*

4.3.1. *Temperature r.m.s. values*

Figure 11 gives the decay of the centreline temperature r.m.s. values normalized by the excess mean temperature at the orifice $(\overline{T'^2})^{1/2}/\Delta\overline{T}_0$ as a function of the distance x/d from the orifice. Within the zone of flow establishment the temperature fluctuations increase to between 1.3% and 1.7% of the excess mean temperature at the orifice and

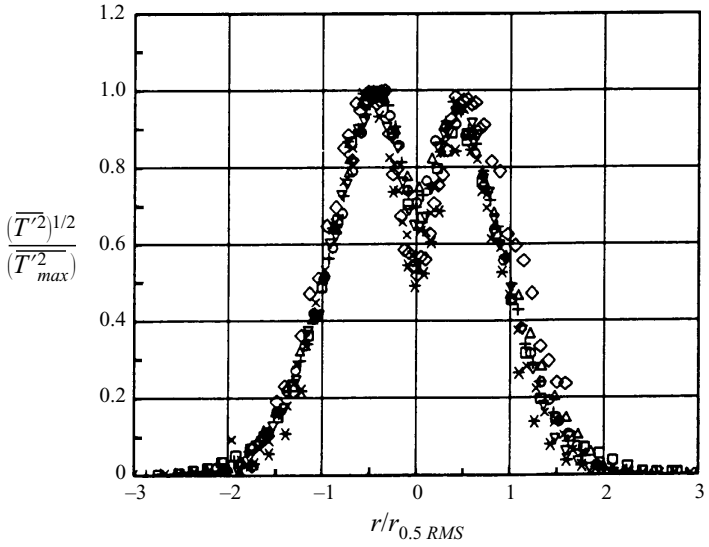

FIGURE 12. Radial profile of the temperature r.m.s. values for the plume.

then they decrease rapidly with further distance from the origin, becoming less than 0.5% at a distance of $x/d = 40$. These figures represent maximum temperature r.m.s. values of 0.5 K for the forced convection jet and the buoyant jet and 1 K for the plume. The minimum values are less than 0.2 K at a distance of $x/d = 40$ for all the measurements made. The decay is proportional to $(x/d)^{-1.1}$ for the forced-convection jet for $x/d \geqslant 11$, and, in the cases of the buoyant jet and the plume, it is proportional to $(x/d)^{-1.2}$ and $(x/d)^{-1.6}$ for $x/d \geqslant 5$. Thus the temperature r.m.s. values decay more rapidly than the mean temperature which always decays proportional to $(x/d)^{-1}$. In contrast, when one considers fluids with higher Prandtl number and normalizes the temperature r.m.s. values on the centreline by the local excess centreline temperature, one finds constant ratios at an axial distance of about $x/d = 40$. Chen & Rodi (1980) give ratios of between 0.21 and 0.26 for jets and 0.39 for plumes, Papanicolaou & List (1987, 1988) give ratios of between 0.15 and 0.22 for jets and 0.40 for plumes. These are in good agreement with experimental findings of Antonia, Prabhu & Stephenson (1975), Grandmaison, Rathgeber & Becker (1977), Birch *et al.* (1978) and Chevray & Tutu (1978) for jets and Nakagome & Hirata (1977) and Kotsovinos (1985) for plumes. The same behaviour is evident in turbulent mass transfer in jets when the concentration r.m.s. values on the centreline are related to the concentration difference between the centreline and ambient. Dahm & Dimotakis (1990) suggest an asymptotic ratio of 0.225, Dowling & Dimotakis (1990) report ratios for various Reynolds numbers in the region of 0.23, Richards & Pitts (1993) give a ratio of 0.227, all for jets dominated by inertia, while Panchapaskesan & Lumley (1993*b*) report an asymptotic ratio of 0.21 to 0.22 for a buoyant jet. The data presented by Ruffin *et al.* (1994) are somewhat lower (asymptotic ratios of about 0.17) but still display asymptotic behaviour. In contrast no asymptotic ratio is observed for sodium and ratios below 0.04 are observed at $x/d = 40$ for all Froude numbers, thus demonstrating the extremely strong damping of the temperature fluctuations due to the high molecular conductivity of sodium.

Figure 12 shows the radial profile of the temperature r.m.s. values $(\overline{T'^2})^{1/2}/(\overline{T'_{max}})^{1/2}$, where $(\overline{T'_{max}})^{1/2}$ is the maximum value, and the radius is normalized by the characteristic half-value radius $r_{0.5RMS}$. Eight profiles for the plume are given and these

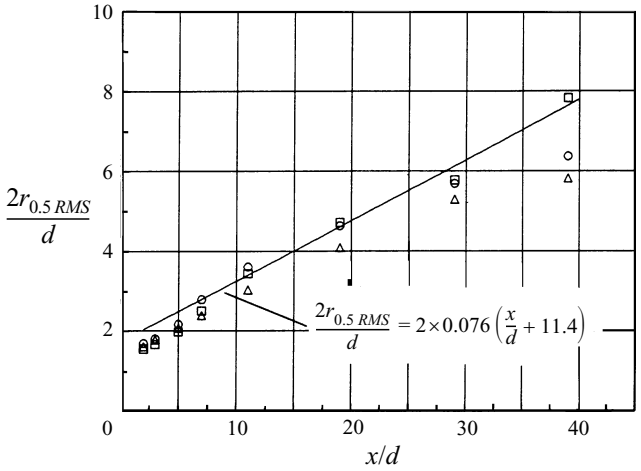

FIGURE 13. Half-value radii of temperature r.m.s. values profiles versus distance from the orifice. □, Forced-convection jet; △, buoyant jet; ○, plume.

are representative of all the measurements made. All profiles are correlated by this single characteristic curve which has two symmetrical maxima of twice the centreline value. Thus, the temperature fluctuations are self-preserving. The maximum r.m.s. value of the temperature fluctuations and the maximum gradient of the mean temperature are at the same radial position $r = r_{0.5RMS}$. Profiles with two maxima are also presented for concentration fluctuations in turbulent jets (Dowling & Dimotakis 1990; Richards & Pitts 1993; Panchapakesan & Lumley 1993) but the maxima are much less pronounced with the peak values no more than 25% higher than the centreline values. According to George, Alpert & Tamanini (1976), the shape of the curve can be explained by the production term $P_t = -\overline{u'T'}\partial\bar{T}/\partial x - \overline{v'T'}\partial\bar{T}/\partial r$ in the transport equation for the temperature fluctuations. For the sodium flows investigated, the second term is always dominant as the radial gradient of the mean temperature is always greater than the axial gradient. An increasing importance of the first term with decreasing Froude number and the formation of a bell-shaped curve for plume flow, as reported by Shabbir & George (1994), is not observed when the temperature field is dominated by molecular diffusion.

The half-value radii for the temperature r.m.s. values $2r_{0.5RMS}/d$, defined as the radius at which the temperature r.m.s. value is half its maximum value, are given in figure 13 as a function of the distance x/d from the orifice. The forced-convection jet data are linear for distances of $x/d \geqslant 11$ with a spreading rate $S_{RMS} = 0.076$. This is in good agreement with the spreading rate for the mean temperature ($S_T = 0.077$), which is to be expected since the diffusion of mean temperature and the temperature fluctuations is governed by the same mechanism in sodium. The data for the buoyant jet and the plume show the same nonlinear behaviour as the data for the mean temperature.

4.3.2. *Statistical properties*

The strong influence of the molecular diffusivity on the temperature field, which is the main difference between sodium and fluids with higher Prandtl numbers, becomes obvious when looking at the statistical properties of the temperature fluctuations. Probability density functions (PDFs) are obtained using a sampling rate of 289 Hz, a value chosen to be significantly higher than the frequency response for the

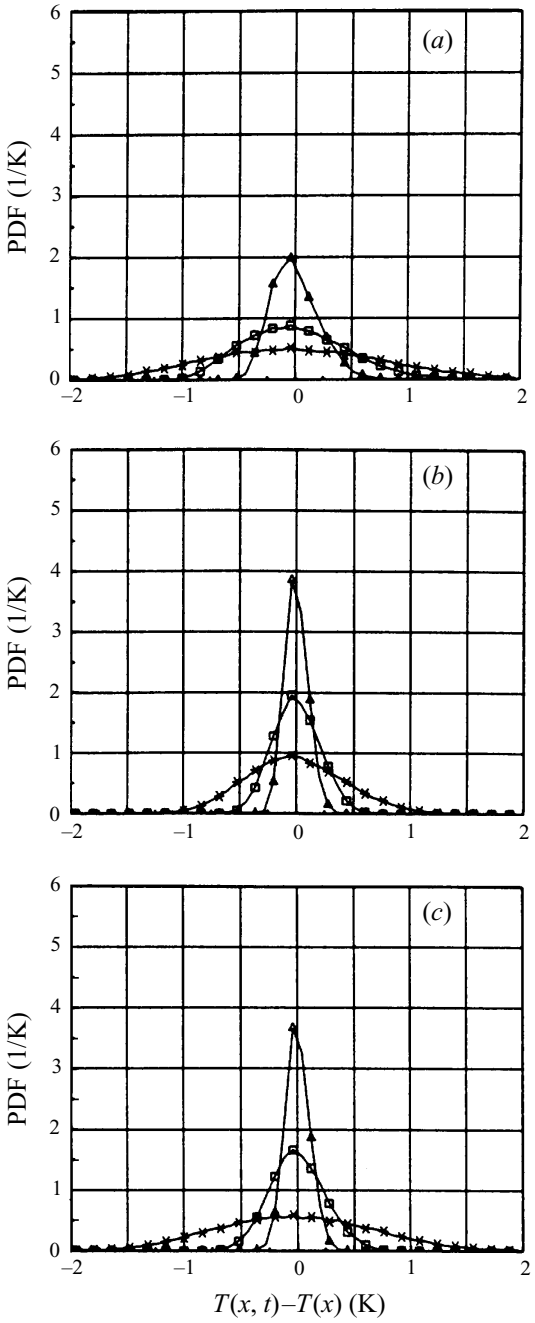

FIGURE 14. Probability density functions for the temperature fluctuations at $r/r_{0.5RMS} = -0.5$ and $x/d = 8$ (□), 20 (△) and 40 (*): (*a*) forced-convection jet, (*b*) buoyant jet, (*c*) plume.

thermocouple but not a multiple of 50 Hz, and they are plotted in figure 14 for the three axial distances $x/d = 8$, 20 and 40. These data are all for $r/r_{0.5RMS} = -0.5$, where the maximum temperature fluctuations are observed. The probability density function for all flows shows a wide distribution at $x/d = 8$, which changes because of smoothing by molecular diffusion to a narrower distribution of small temperature fluctuations

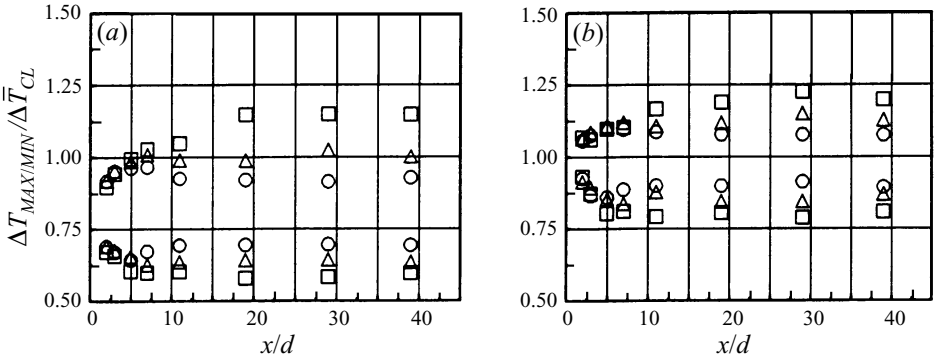

FIGURE 15. Maximum and minimum temperatures versus distance from the orifice at $r/r_{0.5RMS} = -0.5$ (*a*) and $r/r_{0.5RMS} = 0$ (*b*). □, Forced-convection jet; △, buoyant jet; ○, plume.

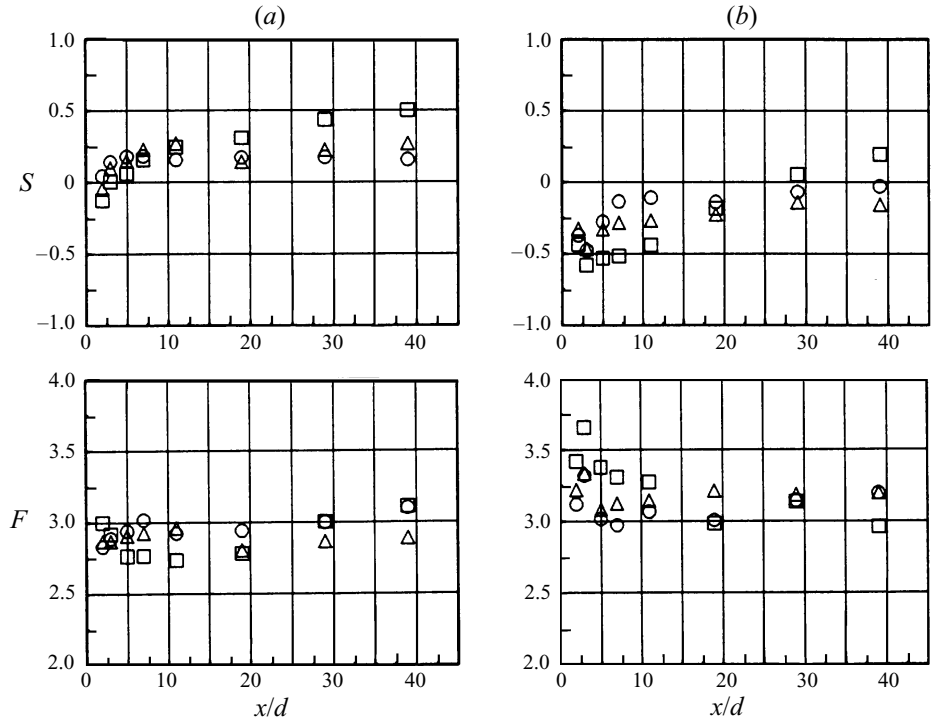

FIGURE 16. Skewness S and flatness F versus distance from the orifice at $r/r_{0.5RMS} = -0.5$ (*a*) and $r/r_{0.5RMS} = 0$ (*b*). □, Forced-convection jet; △, buoyant jet; ○, plume.

around the mean value. Analogously to the decay of the temperature fluctuations in figure 11, which is the steepest with the plume, the greatest change in PDF occurs in the plume flow.

Figure 15 shows the maximum and the minimum temperatures ΔT_{MAX} and ΔT_{MIN} relative to the temperature of the co-flow and normalized by the mean value of the excess centreline temperature $\Delta\bar{T}_{CL}$, plotted against the distance x/d from the orifice. Figure 15(*a*) gives the results at $r/r_{0.5RMS} = -0.5$, and figure 15(*b*) gives the results on the centreline $r/r_{0.5RMS} = 0$. After a zone of flow establishment the maximum and minimum values reach constant levels for all the measurements made. The extreme values along the centreline are within a narrow band of $\pm 20\,\%$ around the mean value.

The extreme values at $r/r_{0.5RMS} = -0.5$ are of the order of 20% below the corresponding values on the centreline, which reflects the decrease in the excess mean temperature in the radial direction. The minimum temperatures at the centreline of 20% below the excess mean temperature mean that there is an intensive heat exchange between the entrained cold fluid of the co-flowing sodium and the hot injected sodium; cold ambient fluid does not penetrate the high-conductivity fluid to reach the axis of symmetry. The heat exchange is enhanced with decreasing Froude number; the difference between maximum and minimum values decreases with decreasing Froude number as can be seen from the decay of the temperature fluctuations in figure 11.

In contrast, the water measurements of Papanicolaou & List (1987) give maximum and minimum values at the centreline that are 50% above and 45% below the excess mean temperature for a forced convection jet. For a plume they find maximum values 150% above the excess mean temperature and minimum values of zero. The low minimum values with water demonstrate clearly the entrainment of cold ambient fluid right to the jet axis without a significant thermal exchange. The maximum values in the water experiments are also much higher than in sodium. A comparison of the behaviour of the two fluids illustrates, first, that the entrained sodium from the co-flow is rapidly heated up due to molecular diffusion and, second, that high, positive temperature fluctuations are damped in the sodium plume by the same process, something which is not found in the water experiments.

The probability density functions in figure 14 do not show major differences from a Gaussian distribution and the values of the skewness S and the flatness F in figure 16 support this observation. Figure 16(a) gives the results at $r/r_{0.5RMS} = -0.5$, and figure 16(b) gives the results on the centreline $r/r_{0.5RMS} = 0$. A signal with a Gaussian distribution has a skewness of $S = 0$ and a flatness of $F = 3$ and, downstream of a zone of flow establishment, the values for the skewness and the flatness differ only slightly from those of a Gaussian distribution. The only difference is that the skewness at $r = -0.5r_{0.5RMS}$ has a tendency towards positive values. This is due to large positive temperature fluctuations (from the jet axis) which are not matched by negative fluctuations of a similar magnitude (from the co-flow), the latter having to migrate over a rather greater distance of the high-conductivity fluid. This can be seen from the maximum and minimum temperatures in figure 15 which are not completely symmetrical about the mean temperature (which corresponds to a value of 0.8 on the y-axis). The negative skewness at the centreline for small axial distances from the orifice is due to elements of cold fluid which are transported to the centreline because of the strong entrainment in the shear layer of the buoyant jet. The negative skewness corresponds to a value of the flatness in excess of 3.

The temperature fluctuations may also be interpreted using the power spectral density S_{TT}. In order to find the frequency response of the thermocouples one measurement is made at an axial distance of $x/d = 3$ and at a radial position of $r/r_{0.5RMS} = -0.5$ because at this position, the highest frequencies with high spectral energy are observed. This measurement gives a constant spectral energy up to frequencies of 40 Hz in sodium and thus the thermocouples are able to detect frequencies up to 40 Hz without any signal attenuation, see figure 17.

Figure 18, which gives the power spectral density of the plume at a radial position of $r/r_{0.5RMS} = -0.5$ and at the three axial distances $x/d = 8$, 20 and 40, is representative of all the measurements made. The power spectral density is approximately constant for frequencies below a particular value, here denoted the break frequency. At higher frequencies there is a narrow convective subrange, in which the temperature eddies are stretched with a slope of $-5/3$. The break frequency decreases with increasing distance

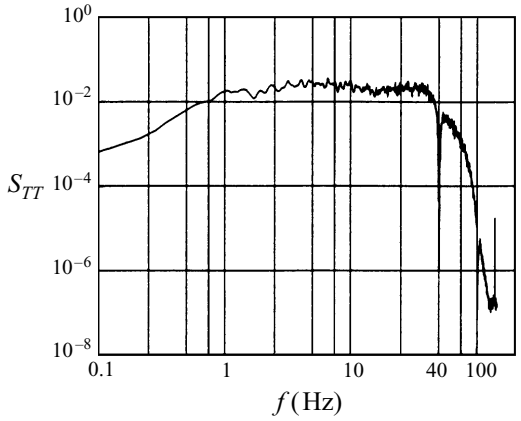

FIGURE 17. Power spectral density at $r/r_{0.5RMS} = -0.5$ and $x/d = 3$ for the plume.

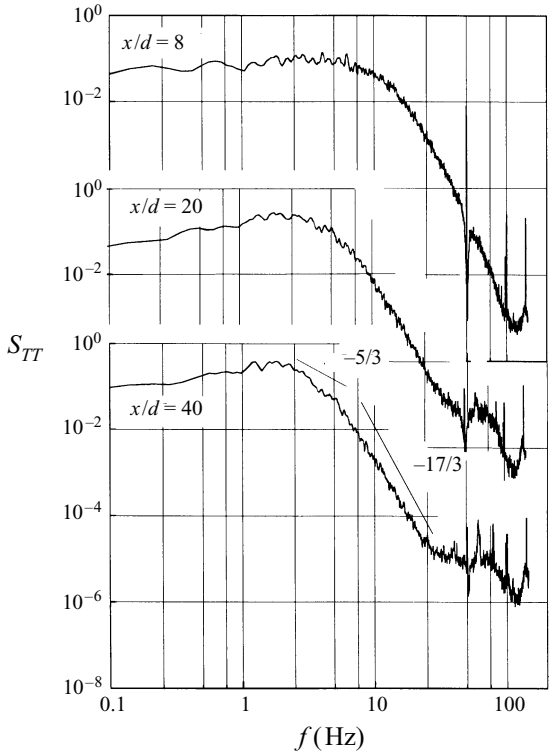

FIGURE 18. Power spectral density at $r/r_{0.5RMS} = -0.5$ and $x/d = 8$, 20 and 40 for the plume.

from the orifice and the convective subrange is enlarged. For even higher frequencies there is a conduction subrange with a slope of $-17/3$, the frequency at which the transition from the convective to the conduction subrange takes place being called the conduction cut-off frequency. The existence of a conduction cut-off frequency is discussed theoretically by Batchelor (1959) and Batchelor *et al.* (1959) for fluids of small Prandtl number. Heat transfer measurements of Bunschi (1976) in sodium also show the narrow convection subrange and the $-17/3$ decay in the conduction subrange. On the other hand temperature measurements in water plumes by Mizushima

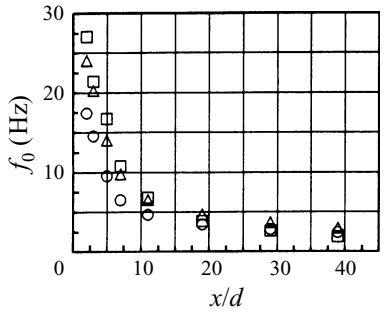

FIGURE 19. Break frequency versus distance from the orifice at $r/r_{0.5RMS} = -0.5$. □, Forced-convection jet; △, buoyant jet; ○, plume.

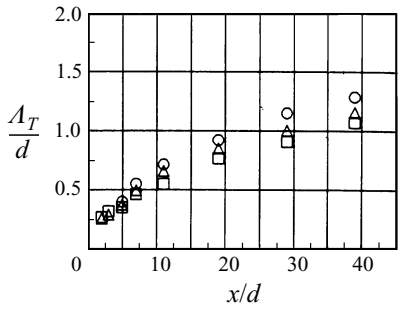

FIGURE 20. Integral length scale versus distance from the orifice at $r/r_{0.5RMS} = -0.5$. □, Forced-convection jet, △, buoyant jet, ○, plume.

et al. (1979), Ramaprian & Chandrasekhara (1983) and Papanicolaou & List (1987) show that the power spectral density first has an inertial-convective subrange with a $-5/3$ decay and then this is followed by a -3 decay for higher frequencies.

Figure 19 gives the break frequency f_0 versus the distance x/d from the orifice at a radial position of $r/r_{0.5RMS} = -0.5$. The break frequency decreases with increasing distance from the orifice and it takes an asymptotic value of 2.5 Hz. The forced-convection jet gives the highest values for small distances from the orifice; this is caused by the high excess velocity which generates a strong entrainment process and hence a high exchange of cold and hot fluid eddies at the measurement position.

4.4. *Turbulence length scales*

The integral length scale Λ_T of the temperature fluctuations, using Taylor's hypothesis (Taylor 1938), is shown in figure 20 as a function of the axial distance x/d from the orifice at a radial position of $r/r_{0.5RMS} = -0.5$. The integral length scale increases with increasing distance from the orifice as larger coherent structures are allowed to develop and these structures can be seen to be larger in a plume than in a forced-convection jet. Papanicolaou & List (1987) confirm the same trends in water. However, Becker, Hottel & Williams (1967), Shaughnessy & Morton (1977) and Birch *et al.* (1978) find integral length scales with concentration measurements in jets of air and methane that are larger than those reported here for temperature fluctuations in sodium. Ruffin *et al.* (1994) also report larger turbulence length scales, in their case of about 0.1 x/d for turbulent velocity fluctuations. The length scales for the temperature fluctuations in the sodium near the jet orifice are about half this size and those farther downstream are proportionately smaller. Since the velocity fields in the sodium jets are consistent with those for fluids of higher Prandtl number, one can conclude that the integral length

scales for the temperature fluctuations are signficantly smaller than those for the velocity fluctuations.

The Kolmogorov turbulence length scales are much smaller; calculations using the data of Ruffin *et al*. (1994) suggest values on the centreline of the forced jet which vary from 9 μm at $x/d = 3$ to 124 μm at $x/d = 40$. According to Lawn (1977) the Kolmogorov length scales for temperature fluctuations in liquid metals are greater by a factor $Pr^{-3/4}$, which gives length scales on the centreline for the forced-convection jet of 0.4 mm at $x/d = 3$, 1.5 mm at $x/d = 10$, 2.9 mm at $x/d = 20$ and 5.8 mm at $x/d = 40$. Hence except, perhaps, for positions very close to the jet nozzle, the 0.25 mm thermocouple will capture the essential features of the temperature fluctuations.

4.5. *Influence of experimental conditions*

The experimental results show some significant differences from the free jet behaviour of fluids of higher Prandtl number. However, the present experimental arrangement departs in a number of respects from the configuration of a classical jet, in which a stream of uniform velocity is injected into a semi-infinite quiescent fluid, and the influence of the experimental configuration will be considered next.

The initial jet velocity profile was that of a fully developed pipe flow. Dahm & Dimotakis (1990) recommend that, in analysing jet data, a source diameter d^*, rather than the nozzle diameter d, should be used where the velocity profile is non-uniform and density differences exist, with d^* calculated from

$$d^* = \frac{2\dot{m}_0}{(\rho_a \pi M_0)^{1/2}} \tag{19}$$

where $\dot{m}_0$ is the initial mass flow rate of the jet and M_0 is its initial momentum flux. If the seventh-root velocity profile (for fully developed pipe flow) is assumed for the present arrangment it can be shown that

$$d^* = d\left(\frac{49\rho_0}{50\rho_a}\right)^{1/2}. \tag{20}$$

The density ρ_0/ρ_a is 1 for the isothermal jet, 0.99 for the forced-convection jet and the buoyant jet and 0.98 for the plume and so the largest correction to the diameter implied by equation (20) is 2 %. Hence the use of the nozzle diameter in analysing data does not lead to significant errors.

In the experiment the sodium jet emerges from a 7.2 mm nozzle into a pipe of 110 mm diameter and therefore the jet is not unrestrained in the classical sense. The experimental results of Steward & Guruz (1977) and the earlier work by Craya & Curtet (1955) and Curtet (1958) suggest that for the range of Craya–Curtet numbers in the sodium experiment (1.5 to 7.2) the pipe wall itself would have little impact on the decay or spreading rates of the velocity and temperature fields. This assertion is supported by the experimental velocity profiles in the pipe at large x/d; even at $x/d = 40$ the velocities outside a central core of 70 mm diameter are uniform.

However, the magnitude of the co-flow influences the jet characteristics, in particular the spreading rate, and especially with the plume where the initial excess velocity of the jet of 0.17 m s^{-1} is of a similar order to the co-flow velocity of 0.1 m s^{-1}. It can be shown using information presented by Rodi (1972) that the centreline velocity decay for the isothermal jet and the forced-convection jet will essentially display classical free-jet behaviour. Furthermore, if density differences are ignored, the axial location corresponding to $x/d = 40$ with the buoyant jet is still within the zone where the centreline velocity decays as $(x/d - x_0/d)^{-1}$. The centreline velocity of the plume is

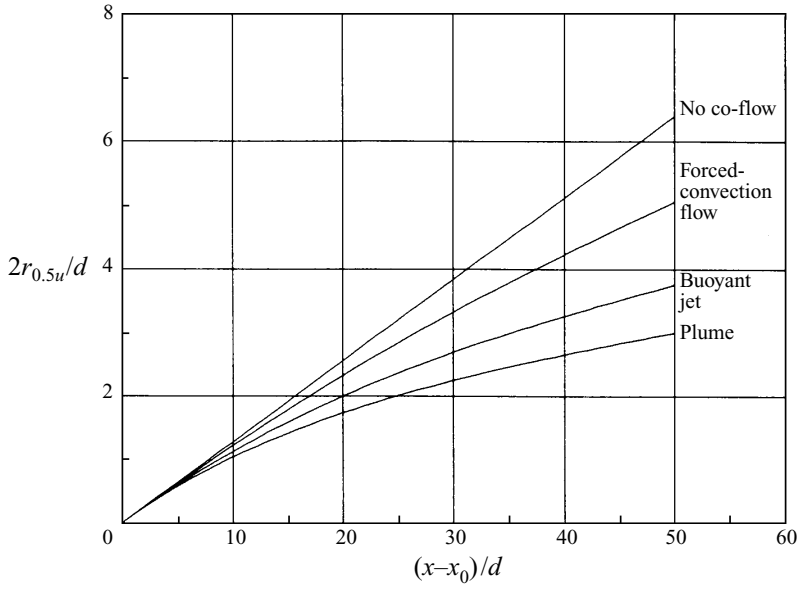

FIGURE 21. Predictions of half-value radii of velocity from Reichardt (1964).

predicted to be affected rather more; at $x/d = 40$ the velocity would be of the order of 10% higher than for a classical jet. Thus the existence of the co-flow accounts in part for the discrepancy between the experimental value of B_u in equation (11) and the lower values for plumes reported in other studies. In contrast, the impact of the co-flow on spreading rates is much more significant, as shown by curves obtained from an expression derived by Reichardt (1964). These are plotted in figure 21 and they are calculated using the appropriate jet outlet velocities and co-flow velocities of the experiment but do not take the effect of buoyancy into consideration. It can be seen that the co-flow is predicted to reduce the width of the buoyant jet at $x/d - x_0/d = 45$ to about 75% of the value for the forced-convection jet and the width of the plume by a further 15%. The differences between the spreading rates observed experimentally are somewhat smaller and the curvature in the distributions predicted by both Reichardt (1964) and Rodi (1972) is not evident. It may therefore be deduced that buoyancy increases the half-value radius of velocity, particularly at large x/d where buoyancy forces have the most significance (this reduces the curvature in the profiles), and that in the present investigation the influence of buoyancy is masked by the restricting effect of the co-flow.

4.6. *Similarity analysis*

Experimental information on the velocity field is generally in agreement with the data for fluids of higher Prandtl number, particularly for the cases where the influence of buoyancy and the co-flow are small. The decay of the centreline temperature is also similar to that in more conventional fluids under conditions of forced convection but it is different in the buoyant jet and the plume. The reasons for this temperature behaviour may be deduced from the similarity analysis of Chen & Rodi (1980) in which it is assumed that the diffusion of both heat and momentum in jets is governed by turbulent processes. Now, in liquid sodium jets the diffusion of heat takes place largely on a molecular scale. Replacing the turbulent heat flux in the energy equation in the similarity analysis

$$q_t = \rho c_p \overline{v'T'} \tag{21}$$

by Fourier's law for conduction

$$q_m = -\rho c_p \alpha \frac{\partial T}{\partial r}, \tag{22}$$

where α is the thermal diffusivity, it can be shown that the similarity analysis remains valid for cases where the buoyancy term in the momentum equation is negligible. The velocity and temperature half-value radii are proportional to the axial distance x, and the centreline velocity and the centreline temperature decay as the reciprocal of x, as in other fluids. This predicted behaviour is consistent with the experimental observations. However, when the buoyancy term $\beta g \Delta T$ in the momentum equation is significant, as is the case for the buoyant jet and the plume, then the similarity breaks down. This is evident from the experimental values of the temperature half-value radii (see figure 9), which do not increase linearly with x for the buoyant jet and the plume. It should also be noted that the similarity analysis assumes the same length scale for the radial variation of velocity and temperature. This is not necessarily the case for liquid metals, in which the temperature variation could extend somewhat farther into the flow than the velocity variation and hence the similarity analysis is more appropriate for fluids with a Prandtl number of the order of unity than for sodium.

4.7. *Transferability of data*

In summary, the velocity fields in the sodium jets show similarities to the velocities in jets of fluids of higher Prandtl number, but the variation of time-mean temperature and the description of the temperature fluctuations (both in terms of the intensity and the length scale) are significantly different, especially for buoyancy-influenced flows. A similar picture is seen for turbulent mixed convection in a vertical pipe, where the distortion of the velocity profile by buoyancy forces in sodium (Jackson *et al.* 1994) is similar to the effect of buoyancy on velocities in other fluids (Jackson, Cotton & Axcell 1989) while the heat transfer behaviour is quite different. In the past, measurements have been made of temperature fluctuations produced by coaxial sodium jets of different temperatures and there is interest in the penetration of such temperature fluctuations through boundary layers, the application being thermally induced fatigue in fast reactor structures (see, for example, Buffet & Tenchine 1985 and Tenchine 1987). Similar measurements have been made in air and water but it is difficult to see how heat transfer data for buoyant flows in simulant fluids can be transferred directly to the reactor application when the thermal descriptions are different in so many respects. The value of experiments in a simulant fluid would therefore appear to be the acquisition of data about the likely velocity field in sodium. Similar experiments in sodium and simulant fluids also permit an examination of the performance of turbulence models in fluids of differing Prandtl numbers, which can produce models of greater universality.

5. Conclusions

The present work investigates, for the first time, the development of a turbulent buoyant sodium jet discharging into a slowly moving pipe flow over a wide range of densimetric Froude numbers. The measurements are possible because of the recent development of a temperature-compensated miniature permanent-magnet flowmeter probe. The measuring principle is based on electro-magnetic induction and, despite an outer diameter of only 2.5 mm, the probe has a very high sensitivity of 47 $\mu V/(m\ s^{-1})$.

The development of buoyant jets in fluids of Prandtl number greater than or equal to 0.7 is well known. The present experimental study extends the data base to include liquid metals, which have very low Prandtl numbers, and helps to define the influence of a low-Prandtl-number fluid on buoyant flow characteristics. The development of a turbulent buoyant sodium jet can be divided into three regions, defined by the non-dimensionalized distance x^* of equation (13), which depends on the densimetric Froude number at the orifice. For large Froude numbers ($x^* < 0.8$) one finds inertia-controlled jet characteristics, for low Froude numbers ($x^* > 5$) one finds buoyancy-controlled plume characteristics, while the transition region ($0.8 < x^* < 5$) may be described as a buoyant jet. As with classical jets, the axial velocity and temperature profiles can be correlated by Gaussian curves. All radial profiles of the temperature r.m.s. values can be correlated by a single curve having a local minimum at the centreline and two very pronounced maxima on either side of it and so the intensity of the temperature fluctuations is also self-preserving.

Generally, the velocity fields in buoyant sodium jets are similar to those in buoyant jets of more common fluids such as water or air. The decay laws for the mean centreline velocity in sodium are in good agreement with the findings for fluids of higher Prandtl number both in the decay constants and in the x/d-dependency. The similarity laws for velocity in the forced-convection jet and the plume are observed. The half-value radius of the mean velocity increases linearly with the axial distance from the orifice for all three regimes. Buoyancy forces tend to increase the spreading rates, although in the present investigation the influence of buoyancy is masked by the effect of the co-flow, which restricts the growth of the jet and therefore acts in the opposite direction.

The momentum flux of the isothermal jet and the forced-convection jet is nearly constant with increasing distance from the orifice. In contrast, the momentum flux for the plume increases linearly from the orifice. For a buoyant jet in the transition region the momentum flux is approximately constant up to a distance corresponding to $x^* = 0.8$ (the limiting value for inertia-controlled jets) and then it increases linearly for larger distances from the origin.

In contrast to the velocity fields, the temperature fields are quite different from those in conventional fluids because, in sodium, heat transfer is dictated by molecular diffusion rather than turbulent diffusion. The decay of the mean centreline temperature is always proportional to $(x/d)^{-1}$ and the half-value radii of the mean temperature do not increase linearly with axial distance for the buoyant jet or the plume. The latter observation confirms that there is no similarity solution when the temperature field in a buoyant jet is dominated by molecular diffusion at the same time as the velocity field is dominated by turbulent diffusion. The temperature fluctuations vary more rapidly in both axial and radial directions than with other fluids, a consequence of the ability of sodium to reduce temperature inhomogeneities. An increase in the temperature r.m.s. values at the centreline resulting from a production of temperature fluctuations by buoyancy forces is not observed. The maximum and minimum excess temperatures on the centreline are in a band of $\pm 20\%$ about the mean temperature, a considerably smaller variation than with fluids of higher Prandtl number. The strong influence of the low Prandtl number of sodium is also evident from the power spectral density, which shows a narrow convective subrange with a $-5/3$ decay followed by a conduction subrange with a $-17/3$ decay.

REFERENCES

Antonia, R. A., Prabhu, A. & Stephenson, S. E. 1975 Conditionally sampled measurements in a heated turbulent jet. *J. Fluid Mech.* **72**, 455–480.

Axcell, B. P. & Walton, A. 1993 Thermoelectric effects in miniature permanent magnet probes used for velocity measurement in flowing sodium. *Expl Thermal Fluid Sci.* **6**, 309–323.

Baker, C. B., George, W. K. & Taulbee, D. B. 1982 An analysis of the axisymmetric turbulent buoyant jet. *Proc. 7th Intl Heat Transfer Conf., Munich*, Paper EN1, vol. 2, pp. 383–388.

Batchelor, G. K. 1959 Small-scale variation of convected quantities like temperature in turbulent fluid. Part 1. General discussion and the case of small conductivity. *J. Fluid Mech.* **5**, 113–133.

Batchelor, G. K., Howells, I. D. & Townsend, A. A. 1959 Small-scale variation of convected quantities like temperature in turbulent fluid. Part 2. The case of large conductivity. *J. Fluid Mech.* **5**, 134–139.

Becker, H. A., Hottel, H. C. & Williams, G. C. 1967 The nozzle-fluid concentration field of the round turbulent free jet. *J. Fluid Mech.* **30**, 285–303.

Birch, A. D., Brown, D. R., Dodson, M. G. & Thomas, J. R. 1978 The turbulent concentration field of a methane jet. *J. Fluid Mech.* **88**, 431–449.

Bremhorst, K. & Krebs, L. 1989 Turbulent Prandtl number in liquid sodium from measurements of mean velocity and temperature in a heated jet. *Proc. 4th Intl Topical Meeting on Nuclear Reactor Thermal-Hydraulics, Karlsruhe, FR Germany*, pp. 764–768.

Bremhorst, K. & Krebs, L. 1992 Experimentally determined turbulent Prandtl numbers in liquid sodium at low Reynolds numbers. *Intl J. Heat Mass Transfer* **35**, 351–359.

Bremhorst, K., Krebs, L., Müller, U. & Listijino, J. H. B. 1989 Application of a gradient diffusion and dissipation time scale ratio model for prediction of mean and fluctuating temperature fields in liquid sodium downstream of a multi-bore jet block. *Intl J. Heat Mass Transfer* **32**, 2038–2046.

Buffet, J. C. & Tenchine, D. 1985 Transfer of temperature fluctuations across boundary layers in turbulent liquid metal flows. *Proc. 1985 Pressure Vessels and Piping Conference, New Orleans, USA, June 23–26, 1985*, pp. 153–157. ASME Materials Division, New York.

Bunschi, H. 1976 Turbulente Temperaturschwankungen in flüssigem Natrium, PhD thesis 5890, Eidgenössische Technische Hochschule, Zürich, Schweiz.

Chen, C. J. & Rodi, W. 1975 A review of experimental data of vertical turbulent buoyant jets. *Rep.* SFB 80/T/69. Universität Karlsruhe.

Chen, C. J. & Rodi, W. 1980 *Turbulent Buoyant Jets – A Review of Experimental Data*. HMT Vol. 4, Pergamon Press.

Chevray, R. & Tutu, N. K. 1978 Intermittency and preferential transport of heat in a round jet. *J. Fluid Mech.* **88**, 33–160.

Corrsin, S. 1943 Investigation of flow in an axially symmetric heated jet of air. *NACA Wartime Rep.* W-94.

Corrsin, S. & Uberoi, M. S. 1949 Further experiments on the flow and heat transfer in a heated turbulent air jet. *NACA TN* 865.

Craya, A. & Curtet, R. 1955 Sur l'evolution d'un jet en espace confiné. *C.R. Acad. Sci. Paris* **241**, 621–622

Curtet, R. 1958 Confined jets and recirculation phenomena with cold air. *Combust. Flame* **2**, 383–411.

Dahm, W. J. A. & Dimotakis, P. E. 1990 Mixing at large Schmidt number in the self-similar far field of turbulent jets. *J. Fluid. Mech.* **217**, 299–330.

Dowling, D. R. & Dimotakis, P. E. 1990 Similarity of the concentration field of gas-phase turbulent jets. *J. Fluid. Mech.* **218**, 109–141.

Fischer, H. B., List, E. J., Koh, R. C. Y., Imberger, J. & Brooks, N. H. 1979 *Mixing in Inland and Coastal Waters*. Academic.

Fuchs, H. 1972 Wärmeübergang an strömendes Natrium, PhD thesis 5110, Eidgenössische Technische Hochschule, Zürich, Schweiz.

George, W. K., Alpert, R. L. & Tamanini, F. 1976 Turbulence measurements in an axisymmetric plume. *Factory Mutual Research Rep.* 22359-2. Factory Mutual System, Norwood, MA 02062, USA.

Grandmaison, E. W., Rathgeber, D. E. & Becker, H. A. 1977 Some characteristics of concentration fluctuations in free turbulent jets. *Proc. 1st Symp. on Turbulent Shear Flows*, *Penn. State Univ.*, pp. 5.21–5.29.

Horanyi, S. & Krebs, L. 1986 Experimental investigations of temperature fluctuations in subchannels of sodium cooled 4 rod bundle TEGENA. In *Pressure and Temperature Measurements*, HTD-Vol. 58, pp. 5–44. ASME.

Horanyi, S. & Krebs, L. 1988 Temperature compensated miniature permanent magnet flowmeter for liquid metal. *Proc. 1st World Conf. Experimental Heat Transfer, Fluid Mechanics and Thermodynamics*, *Sept. 4—9*, *Dubrovnik*, *Yugoslavia*, pp. 279–285.

Hussein, H. J., Capp, S. P. & George, W. K. 1994 Velocity measurements in a high-Reynolds-number, momentum-conserving, axisymmetric, turbulent jet. *J. Fluid Mech.* **258**, 31–75.

Jackson, J. D., Axcell, B. P. & Walton, A. 1994 Mixed-convection heat transfer to Sodium in a vertical pipe. *Expl Heat Transfer* **7**, 71–90.

Jackson, J. D., Cotton, M. A. & Axcell, B. P. 1989 Studies of mixed covection in vertical tubes. *Intl J. Heat Fluid Flow* **10**, 2–15.

Knebel, J. U. 1993 Experimentelle Untersuchungen in Turbulenten Auftriebsstrahlen in Natrium. PhD thesis, Universität Karlsruhe and *KfK-Rep.* 5175, Kernforschungszentrum Karlsruhe, Germany.

Knebel, J. U. & Krebs, L. 1993 Kalibrierung einer Miniatur-Permanentmagnet-Potentialsonde zur Geschwindigkeits- und Temperaturmessung in Natrium. *KfK-Rep.* 5215. Kernforschungszentrum Karlsruhe, Germany.

Knebel, J. U. & Krebs, L. 1994 Calibration of a miniature permanent magnet flowmeter probe and its application to velocity measurements in liquid sodium. *Expl Thermal Fluid Sci.* **8**, 135–148.

Knebel, J. U., Krebs, L. & Müller, U. 1993 Experimental investigations on the velocity and temperature field in axi-symmetric turbulent buoyant jets of sodium. *Proc 9th Symp. on Turbulent Shear Flows*, *Kyoto*, *Japan*, pp. 12.2.1–12.2.6.

Kotsovinos, N. E. 1985 Temperature measurements in a turbulent round plume. *Intl J. Heat Mass Transfer* **28**, 771–777.

Kotsovinos, N. E. & Angelidis, P. B. 1991 The momentum flux in submerged jets. *J. Fluid Mech.* **229**, 453–470.

Krebs, L. & Bremhorst, K. 1983 Verification of the extended gradient diffusion model by measurement of the mean and fluctuating temperature fields in sodium flow downstream of a multi-bore jet block. *Proc. 4th Symp. Turbulent Shear Flows*, *Karlsruhe*, *Germany*, pp. 17.1–17.5.

Lawn, C. J. 1977 Turbulent temperature fluctuations in liquid metals. *Intl J. Heat Mass Transfer* **20**, 1035–1044.

List, E. J. 1982*a* Turbulent jets and plumes. *Ann. Rev. Fluid Mech.* **14**, 189–212.

List, E. J. 1982*b* Mechanics of turbulent buoyant jets and plumes. In *Turbulent Buoyant Jets and Plumes* (ed. W. Rodi), pp. 1–68. Pergamon.

Mizushina, T., Ogino, F., Veda, H. & Komori, S. 1979 Application of laser-Doppler velocimetry for turbulence measurement in non-isothermal flow. *Proc. R. Soc. Lond.* A **366**, 63–79.

Morton, B. R. 1959 Forced plumes, *J. Fluid Mech.* **5**, 151–163.

Müller, St. & Thun, G. 1977 Permanentmagnetische Durchflußmesser-Sonde für flüssige Metalle. *KfK-Rep.* 2429. Kernforschungszentrum Karlsruhe, Germany.

Müller, St. & Thun, G. 1980 Performance of permanent magnet flowmeter probes for instrumentation of LMFBR's. *Proc. 2nd Intl Conf. Liquid Metal Technology in Energy Production*, *Richland*, *Washington*, *USA*, pp. 4-44–4-51.

Nakagome, H. & Hirata, M. 1977 The structure of turbulent diffusion in an axi-symmetrical thermal plume. *Proc. 1976 ICHMT Seminar on Turbulent Buoyant Convection*, pp. 361–372. Hemisphere.

Ogino, F., Takeuchi, H., Kudo, I. & Mizushina, T. 1980 Heated jet discharged vertically into ambient of uniform and linear temperature profile. *Intl J. Heat Mass Transfer* **23**, 1581–1588.

Panchapakesan, N. R. & Lumley, J. L. 1993*a* Turbulence measurements in axisymmetric jets of air and helium. Part 1. Air jet. *J. Fluid Mech.* **246**, 197–223.

Panchapakesan, N. R. & Lumley, J. L. 1993*b* Turbulence measurements in axisymmetric jets of air and helium. Part 2. Helium jet. *J. Fluid Mech.* **246**, 225–247.

Papanicolaou, P. N. & List, E. J. 1987 Statistical and spectral properties of tracer concentration in round buoyant jets. *Intl J. Heat Mass Transfer* **30**, 2059–2071.

Pananicolaou, P. N. & List, E. J. 1988 Investigations of round vertical turbulent buoyant jets. *J. Fluid Mech.* **195**, 341–391.

Ramaprian, B. R. & Chandrasekhara, M. S. 1983 Study of vertical plane turbulent jets and plumes. *IIHR Rep.* 257. Iowa Institute of Hydraulic Research.

Reichardt, H. 1964 Turbulente Strahlausbreitung in gleichgerichteter Grundströmung. *Forsch. Ing.-Wes.* **30/5**, 133–139.

Reimche, W., Stegemann, D. & Montes, M. 1985 Velocity profile and flow measurements in liquid sodium by signal correlation flowmeters. *Prog. Nucl. Energy* **15**, 727–734.

Richards, C. D. & Pitts, W. M. 1993 Global density effects on the self-preservation behaviour of turbulent free jets. *J. Fluid. Mech.* **254**, 417–435.

Ricou, F. P. & Spalding, D. B. 1961 Measurements of entrainment by axisymmetric turbulent jets. *J. Fluid Mech.* **11**, 21–32.

Ricou, R. & Vives, C. 1982 Local velocity and mass transfer measurement in molten metals using an incorporated magnet probe. *Intl J. Heat Mass Transfer* **25**, 1579–1588.

Rodi, W. 1972 The prediction of free turbulent boundary layers by use of a two-equation model of turbulence. PhD thesis, Imperial College, University of London.

Ruffin, E., Schiestal, R., Anselmet, F., Amielh, M. & Fulachier 1994 Investigation of characteristic scales in variable density turbulent jets using a second-order model. *Phys. Fluids* **6**, 2785–2799.

Rust, K., Weinberg, D., Hoffmann, H., Hain, K., Frey, H. H., Baumann, W., Hayafune, H. & Ohira, H. 1995 Summary report of steady state NEPTUN investigations into passive decay heat removal by natural convection. *Wissenschaftliche Berichte FZKA* 5665.

Schneider, W. 1985 Decay of momentum in submerged jets. *J. Fluid Mech.* **54**, 91–110.

Shabbir, A. & George, W. K. 1994 Experiments on a round buoyant plume. *J. Fluid Mech.* **275**, 1–32.

Shaughnessy, E. J. & Morton, J. B. 1977 Laser light-scattering measurements of particle concentration in a turbulent jet. *J. Fluid Mech.* **80**, 129–148.

Shercliff, J. A. 1987 *The Theory of Electromagnetic Flow Measurement*. Cambridge University Press.

Sheriff, N. & O'Kane, D. T. 1981 Sodium eddy diffusivity of heat measurements in a circular duct. *Intl J. Heat Mass Transfer* **24**, 205–211.

Steward, F. R. & Guruz, A. G. 1977 Aerodynamics of a confined jet with variable density. *Combust. Sci. Technol.* **16**, 29–45.

Takeda, Y. 1986 Velocity profile measurement by ultrasound Doppler shift method. *Intl J. Heat Fluid Flow* **7**, 313–318.

Taylor, G. I. 1938 The spectrum of turbulence. *Proc. Roy. Soc. Lond.* A **164**, 476–490.

Taylor, G. I. 1958 Flow induced by jets. *J. Aero. Sci.* **25**, 464–465.

Tenchine, D. 1987 Thermal-hydraulics of coaxial sodium jets. *AIChE Symp. Series 257*, vol. 83, pp. 151–156.

Walton, A. 1991 Mixed convection heat transfer to sodium in a vertical pipe. PhD thesis, University of Manchester.

Weissenfluh, T. von 1985 Probes for local velocity and temperature measurements in liquid metal flow. *Intl J. Heat Mass Transfer* **28**, 1563–1574.